# An investigation of an underwater steam plasma discharge as alternative to air plasmas for water purification

**Sarah N Gucker[1], John E Foster[1] and Maria C Garcia[2]**

[1] Department of Nuclear Engineering and Radiological Sciences, University of Michigan, Ann Arbor, MI, 48109, USA

[2] Departamento de Física Aplicada, Universidad de Córdoba, Edificio A. Einstein (C-2), Campus de Rabanales, Córdoba 14071, Spain

E-mail: sngucker@umich.edu

## Abstract

An underwater steam plasma discharge, in which water itself is the ionizing media, is investigated as a means to introduce advanced oxidation species into contaminated water for the purpose of water purification. The steam discharge avoids the acidification observed with air discharges and also avoids the need for a feed gas, simplifying the system. Steam discharge operation did not result in pH changes in the processing of water or simulated wastewater, with the actual pH remaining roughly constant during processing. Simulated wastewater has been shown to continue to decompose significantly after steam treatment, suggesting the presence of long-lived plasma-produced radicals. During steam discharge operation, nitrate production is limited, and nitrite production was found to be below the detection threshold of (roughly 0.2 $mgL^{-1}$). The discharge was operated over a broad range of deposited power levels, ranging from approximately 30W to 300W. Hydrogen peroxide production was found to scale with increasing power. Additionally, the hydrogen peroxide production efficiency of the discharge was found to be higher than many of the rates reported in the literature to date.

**Keywords:** plasmas in liquids, plasma water purification, plasma chemistry, plasma generation

## Introduction

The use of atmospheric pressure, non-thermal air plasmas for water sterilization and purification has been an active area of research worldwide [1–4]. These plasmas in laboratory demonstrations have been used to destroy organic contaminants, such as textile dyes [5] and antibiotics in aqueous solutions [6], as well as inactivating biological microorganisms [7]. From an implementation perspective, these air discharges are especially attractive as the working medium is readily available. However, the drawback of the use of air plasmas in liquid water applications is the acidification of the liquid water through the formation of reactive nitrogen species (RNS), such as nitrates, nitrites and peroxynitrites [8]. While creating acidic conditions is a desired effect in certain applications of atmospheric pressure plasma discharges (e.g. antimicrobial treatment is most efficient at pH of 3–4 and lower [9]), if the aim is to process contaminated water for reasonable reuse (by humans, agriculture or industry), the treated liquid must be post-processed to raise the pH. For air-based non-thermal atmospheric plasmas, the primary acidification of the water is thought to be primarily due to the formation of nitrogen and NOx-based species (e.g. nitric acid, among others) [10]. It should be possible to eliminate this acidification pathway by eliminating the nitrogen in the feed gas or using an inert gas as the feedstock. It should be stressed, however, that liquid water still contain trace amounts of dissolved air which is a potential source gas for acidification [11]. Regardless, if the goal is to create a commercially viable and economically feasible

water sterilization system, rare gases such as argon and helium should be avoided. In addition, the use of oxygen gas as the ionizing medium, while eliminating NOx production, presents additional challenges including safety issues. A plasma source presented in this work utilizes the liquid itself as the precursor to the feed gas—water vapor, thereby circumventing the production of $NO_x$. This operation mode, termed 'steam discharge' or 'steam mode', operates such that the treatment liquid becomes the ionized medium fueling the plasma discharge. This no-airflow discharge mode was first examined by Foster et al [12] and has been spectroscopically investigated by Garcia et al [13]. Numerous authors have investigated plasma formation in self-generated steam pockets in saline solutions [14, 15], but this formation takes place in high conductivity solutions (e.g. roughly 1.3 $Sm^{-r}$ in [16]) unlike the deionized water used in this work (10 s of μS $cm^{-m}$). Work by Shih and Locke [17] demonstrated the use of discharge in a steam bubble; however, their discharge was created in boiling water—the steam pocket was not self-generated. Self-generation of a steam pocket within low conductivity water reduces the engineering factors of the system.

**Experimental methods**

The experimental set up, depicted in figure 1, was based on a previously developed underwater dielectric barrier discharge jet [12], with a slight modular adaption to switch between the air mode and the steam mode. The source consisted of a cylindrical copper discharge electrode driven sinusoidally at high voltages (figure 2) that was coaxially positioned within an interchangeable quartz housing (6mm OD, 4mm ID). A coiled copper ground electrode was wrapped around the outside of the quartz discharge tube. The end of the electrode system was positioned

approximately halfway in a 100mL graduated cylinder containing liquid to be treated. All treated liquid maintained a temperature of less than 90 °C. The operating voltage range was 3 and 13 $kV_{p-p,}$ at a frequency of 5 kHz, provided by Elgar 501SL power supply with 50:1 step-up transformer. Voltages were measured with Tektronix 20 kV high voltage probes, and discharge current was measured via 6595 Pearson coil. A 2 GHz oscilloscope (LeCroy Wavepro 7200a) was used to record all associated data (i.e. voltage, etc). For the air mode, room air was pumped at 5.0 SCFH (2.4 $Lmin^{-1}$) through the quartz housing around the inner electrode, exhausting into the liquid to be treated. As previously mentioned, the steam mode self-generates a cavity of water vapor from the water itself, and thus did not require additional feed gas. Power measurements Power deposition was calculated via Lissajous figures for both steam and air discharge operation. Both discharge modes (i.e. steam and air) may be operated between approximately 30 to 300W. As the steam discharge self-generates its own steam pocket, the power deposited in the steam discharge not only vaporizes liquid locally to create the bubble and but it also sustains the plasma. Efficiency between the two methods was calculated using the $G_{50}$ value [2]. Lissajous method Deposited power was determined via the Lissajous figure method, a common and accurate method of power measurement for dielectric barrier discharges [18]. This method was chosen over direct integration of current and voltage waveforms as it avoids error and uncertainty associated with integration of complex waveforms which can lead to the missing of fine structure due to limited oscilloscope bandwidth.

**Power measurements**

Power deposition was calculated via Lissajous figures for both steam and air discharge operation. Both discharge modes (i.e. steam and air) may be operated between approximately 30 to 300W. As the steam discharge self-generates its own steam pocket, the power deposited in the steam discharge not only vaporizes liquid locally to create the bubble and but it also sustains the plasma. Efficiency between the two methods was calculated using the $G_{50}$ value [2].

*Lissajous method*

Deposited power was determined via the Lissajous figure method, a common and accurate method of power measurement for dielectric barrier discharges [18]. This method was chosen over direct integration of current and voltage waveforms as it avoids error and uncertainty associated with integration of complex waveforms which can lead to the missing of fine structure due to limited oscilloscope bandwidth.

*Energy yield*

Estimating energy efficiencies between the two discharge modes was determined through comparison of the $G_{50}$ value [2], or the quantity of destroy pollutant given as

$$G_{50} = \frac{1.8 \times 10^6 C_0 V_0 M}{P t_{50}} \quad (1)$$

where $G_{50}$ is given in grams per kilowatt hour (g kW $h^{-1}$); C0 is the molar concentration of the pollutant at t = 0; $V_0$, the treated volume; M, pollutant molecular weight; P, power in watts; and $t_{50}$, the processing time necessary to remove 50% of the pollutant.

**Baseline studies: DI water**

For comparative purposes, the air and steam discharges were run at comparable discharge voltage and input power settings (~5.5 $kV_{pk-pk}$ and ~60W, respectively) for 4min in deionized water. pH and conductivity measurements were made at regular intervals throughout the treatment to obtain time-resolved evolution of these properties. Immediately after plasma treatment, ion chromatography of the processed liquid was preformed to analyze nitrate ($NO_3^-$) and nitrite ($NO_2^-$) content. These species were chosen as they are precursors to nitric acid formation as described in equation (2) through equation (6) below [10].

$$3NO_2 + H_2O \rightarrow 2H^+ + 2NO_3^- + NO \quad (2)$$

$$NO_2 + OH \rightarrow HNO_3 \quad (3)$$

$$2NO_2(g) \rightarrow N_2O_4(g) + H_2O(l) \rightarrow HNO_3(l) + HNO_2(l) \quad (4)$$

$$NO_2(g) + NO(g) \rightarrow N_2O_3(g) + H_2O(l) \rightarrow 2HNO_2(l) \quad (5)$$

$$3HNO_2(l) \rightarrow HNO_3 + 2NO(g) + H_2O(l) \quad (6)$$

Optical emission spectroscopy of both air and steam discharges was performed to assess the species production and various plasma properties. Hydrogen peroxide formation rates of the steam discharge were measured for various power depositions, and compared to published, plasmas-derived hydrogen peroxide formation rates.

**Decomposition studies: simulated wastewater**

To study the decomposition capability of the steam discharge relative to that air feed source, the sources were both operated in simulated wastewater. In this case, a

solution of methylene blue dye was used as a surrogate for textile mill wastewater, commonly used in plasma decomposition studies [1, 19–21]. It is well established that the textile mill industry is a major contributor to wastewater production and environmental pollution in general [22, 23]. A 100mL solution of 0.1mM methylene blue dye with deionized water was used, treated and analyzed via a spectrophotometer and mass spectroscopy. The starting pH of the solution varied between 5.71 and 6.69, and conductivity of the solution varied between 13 and 100 $\mu Scm^{-1}$.

**Diagnostics**

*Optical*

Optical emission spectroscopy was performed via a.3 m focal length spectrometer with a holographic, 1800 grooves $nm^{-1}$ grating. The slit function was measured via 632.8nm HeNe laser light and correlated with a Gaussian profile of FWHM of 0.14nm. The spectrometer was used in concert with a fast ICCD, capable of 2 ns gating. High-speed photography (Redlake MotionPro HS-4 camera) recorded the steam bubble formation (exposure, 1 μs; frame rate, 200000 fps). A high-speed photodiode (Thorlabs DET210; rise time, 1 ns; 350 MHz operation) was used to analyze the first-light of the discharge.

*Temperature*

The temperature of the high voltage electrode was measured via nickel-chrome high-temperature thermocouple (Super OMEGACLAD XL, ungrounded). Electrode temperature yields insight into the role that the electrode plays in the formation of vapor.

*Sonic verification*

A hydrophone was employed to study the formation and subsequent collapse (cavitation) of locally produced steam bubbles.

*Chemical*

pH and conductivity measurements were performed with a handheld meter (Thermo Scientific Orion Star A329). A spectrophotometer was used to indirectly measure the quantity of MB dye in the liquid, before, during and after treatment. The wavelength setting of the spectrophotometer was 609nm, a strong absorbance peak/region for the dye. For direct measurements of the molecular content, samples were analyzed via ion chromatograph (Dionex DX-100, carbonate eluent). Hydrogen peroxide concentration was determined enzymatically with colorimetric test strips for rapid, in situ H2O2 determination, and via iodometric titration (Hach HYP-1) for post-processing peroxide determination. The iodometric titration method utilizes ammonium molybdate to catalyze the peroxide, and the solution is acidified with sulfite reagent. Potassium iodide reacts with the peroxide to form free iodine and water (see equation (7)). To determine the $H_2O_2$ concentration, sodium thiosulfate titrates the iodine and the quantity of peroxide is calculated (see equation (8)).

$$H_2O_2 + 2KI + H_2SO_4 \rightarrow I_2 + K_2SO_4 + 2H_2O \quad (7)$$

$$I_2 + 2Na_2S_2O_3 \rightarrow Na_2S_4O_6 + 2NaI \quad (8)$$

Hydrogen peroxide is used as a metric for reactive species generation as the formation of hydrogen peroxide is believed to be principally due to the recombination of hydroxyl radicals [24], one of the most important species to plasma purification and treatment [25]. In addition, measuring hydrogen peroxide

formation provides insight for accurate comparison to existing plasma purification devices [26].

**Results: generation of steam bubble**

The self-generation of the steam bubble was studied from several aspects. High-speed photography provided visual confirmation of microbubble structures. Thermocouple studies revealed the steam generation driven by electrode heating was unlikely. Finally, voltage, current, photo detector and acoustic data are used to track the discharge from bubble inception to plasma formation.

*Optical assessment via high speed photography*

To study the origin of the steam bubble, high-speed photography was used. As mentioned in related studies [13], the formation of the steam bubble was studied with a Redlake Motion Pro HS-4 camera. The repetition rate used was 200000 fps, exposure of 1 μs. The physical area imaged by the camera was an 8 × 148 pixel area, or approximately 0.24 × 4.5mm around and below the electrode (see figure 3). Any change, other than slow bubble growth (i.e. bubbles forming on the electrode as in Frame 6 of figure 5), occurs during the early part of the first frame acquired, thereby eliminating the prospect of time resolution at least at early times. This all occurs during the rising edge of the voltage waveform, or on timescales shorter than 1ms). It is possible that the rapidly increasing electric field at early times is sufficient to cause the localized heating responsible for the steam bubble generation. Figure 4 illustrates local variations near the electrode over the voltage cycle. The beginning of each voltage cycle of the first 19 applied voltage cycles is shown figure 5. As can be seen here, evidence of a lower density medium is apparent in frame 6. This mass of presumably steam bubbles grows over the voltage cycle and is ejected into the

liquid at the start of the next voltage cycle. The growth rate of this nascent steam bubble, which grows physically attached to the tip of the electrode (see figure 4), was measured to be approximately 0.33 $ms^{-1}$. Near the electrode bubbles and low-density masses continue to be produced. The index of refraction changes associated with the darkened regions suggested local volume heating. At frame 16, a single steam bubble approximately 65 microns in diameter is observed 1.2mm from the electrode tip. The following images show more bubbles appearing and moving in and out of the frame, starting to form a matrix of bubbles that eventually coalesce into the large, macroscopic bubbles that the discharge occupies.

*Electrode heating*

To investigate the possibility of localized electrode heating of surrounding water, the temperature of the powered electrode was monitored during bubble formation. A high-temperature, ungrounded thermocouple was used to assess temperature of the electrode 10mm away from the tip of the powered electrode. During bubble formation and initial plasma formation, while subjected to high voltage for up to 3 s (the steam bubble had formed within the first 0.05 s, e.g. see figure 6), the temperature of the electrode did not increase above 55 °C.

Because of the high thermal conductivity of copper, it is expected that this temperature should be representative of the temperature at the actual electrode tip. In this regard, localized boiling driven by a electrode heating was ruled out as a the mechanism for bubble formation.

*Development of the steam plasma discharge*

The time evolution of the steam discharge was assessed by measuring charge transfer over a cycle using a sense capacitor, discharge current, photo diode response and resultant power deposition inferred the Lissajous method. The first 0.1 s after the start of application of voltage to the discharge applicator is shown in figure 6. In that figure, $V_1$ is the applied voltage; $V_2$, the voltage across the capacitor; I, the discharge current; and PD, the response from the photo diode. These first moments of the discharge suggest three distinct operating regimes: the Bubble Formation regime, which starts at power application to approximately 0.03 s; the Transition regime which lasts from approximately 0.03 s to 0.045 s; and the Discharge region, which is the region from 0.045 s onward. While each region will be examined more fully in the proceeding paragraphs, an overview of all three regions shown in figure 6 is useful in parsing out the underlying physics of each operating regime. As seen in figure 6, the amplitude of the applied voltage stays roughly constant during the first portion of the Bubble Formation region, while the discharge current very slightly increases. This corresponds to the discharge area (i.e. the growing steam bubble surface area) increasing with current. When the bubble is fully formed, the Transition region begins (at roughly 0.035 s). Here, the discharge current sinks as the applied voltage begins to climb. This is expected as the system transitions into a spark. A discharge spike in the applied voltage is seen at roughly 0.044 s, which is followed by a response from the current, voltage across the capacitor, and photo diode. The remainder of the data (the Discharge region) gives a typical response seen by underwater DBD-type discharges [27]. The power dissipated throughout all three regimes is shown in figure 7 and concisely demonstrates the system shifting from a primarily of liquid conduction and dissipation (the Bubble Formation region, approximately 50W when the power

supply is first turned on) to the plasma discharge regime, where the side slope of the figure are indicative of the capacitance of the dielectric (steam layer and water in this case) (Discharge region, approximately 60W when the discharge is fully ignited).

*Bubble formation*

The first 0.03 s of discharge correspond to the early formation of the steam envelope. This phase may be observed in the first 0.001 s of figure 8. The discharge current is seen to precede the applied voltage, as expected. The phase shift between the discharge current and the applied voltage is 28.3° (I leading V1), and between the applied voltage and the voltage across the capacitor is 78.2° (V1 leading V2). Here, the photodiode response, which is in phase with the applied voltage, is assumed to be pickup noise. The power deposition during the stage as determined via the Lissajous method was approximately 50W, which is enough to vaporize approximately 26.9mg of water per second. This vaporization is believed to fuel the microbubbles at the surface of the electrode and throughout the liquid as seen in figure 5. The Lissajous figure acquired during this early phase is an ellipse (as seen in figures 7 and 9), signifying conduction throughout the cycle. This is observed in conventional DBD discharges operated at high frequency or low pressure. In these cases, the plasma does not decay before a new cycle begins. Charging and discharge effects are not pronounced in this case. In this present case, conductive fluid plays the role of the plasma.

*Transition region—first light*

The transition between the macro-sized steam bubble and actual plasma formation can be inferred from figure 8. A drop in applied voltage is observed around 0.0434

s. This voltage drop is immediately followed by a current spike. Only after the drop in voltage does the photodiode respond, suggesting the breakdown. The power deposition of the Transition region may be seen in the Lissajous figures in figure 9. Power dissipated increases from approximately 71W to 84W as the system switches from bubble formation mode to breakdown. As mentioned previously, the ellipse shaped Lissajous figures are associated with dissipation in the liquid leading to bubble formation. Formation of the vapor barrier and plasma gives rise to a parallelogram shaped. In principal, one Lissajous figure should pass from ellipse to line to parallelogram. The line would indicate full vapor coverage and thus complete isolation of the electrode from the liquid. Absence of the line Lissajous figure suggests that perhaps the electrode is not completely isolated from the liquid; that is, either certain portion of the electrode remain in contact with liquid or a rapidly developing discharge (e.g. corona) may form when coverage is sufficiently high.

*Discharge region*

The section of data shown in figure 10 corresponds to 0.08 to 0.081 s after power was first applied to the electrode, well into the Discharge region of the data. These waveforms are characteristic of the steam discharge while in operation [28]. As with the bubble formation region, the power deposition of this region is roughly constant at approximately 60W (refer to figure 7); overall, the steam discharge is fairly stable in individual regions of operation, with all changes in power associated with changes in operating mode. The fact that the Lissajous figure in this final phase is not exactly rectangular as in figure 9, but rather rounded, suggests that vapor bubble coverage

is not complete or steady and therefore over a cycle, the discharge current is associated with liquid conduction current as well as plasma current.

**Acoustic signal of the steam discharge**

The premise of the discharge formation in low conductivity water is vapor formation at the electrode. Bubbles formed locally at the electrode contain super heated vapor and thus cool rapidly and collapse. The acoustic signature associated with bubble formation and collapse (e.g. [29, 30]) gives a great deal of insight into the bubble formation process as well as subsequent bubble 'tearing' and cavitation once the discharge starts. The acoustic signature for bubble and discharge formation was measured using a miniature-hydrophone. The evolution of the discharge with inclusion of the hydrophone response is shown in figure 11. Pressure pulses or spikes in the hydrophone signal occur with each spike from the photodiode, suggesting a link between plasma generation and the fluid dynamical effects driving sound generation. Possible sources of the acoustic signature include gas heating associated with steamer formation resulting in bubble formation and collapse as seen in [29, 30]. Further analysis of signature is left to future work.

*Summary*

The measurements outlined previously suggest the generation of the steam pocket in deionized water is to be primarily due to electric field-driven processes, such as ion drag, that occur on time scales faster than 1ms. This is opposed to mechanisms such as thermal-driven processes. The formation of the steam bubble is unique in that it is formed in low conductivity water (as opposed to saline solutions, e.g. [31]) and at low frequencies (i.e. not akin to microwave in water as in [31]).

**Results: baseline tests with deionized water**

*pH*

To access the effect of the steam plasma on water pH with that of an air driven plasma, the discharge tube was operated with air as the feed gas in deionized water for four minutes by the air mode. Deionized water was similarly processed with the steam discharge (no input air) for four minutes as well for similar applied voltages (~5.5kV$_{pk-pk}$) and input powers (~60W). During treatment, water samples were extracted periodically to access the time variation in the liquid water's pH. The time resolved variation in the pH is shown in figure 12. The pH of the water treated with air as the feed gas exhibited the expected drop-off in pH with time. After four minutes of processing, the pH of the water treated by the air discharge was approximately 3. This acidification behavior has been reported on extensively [29, 15, 30]. The pH of the water treated in steam mode, however, did not vary appreciably; after four minutes of processing at similar power levels the pH of water remained nearly constant at approximately 6.2. These observations support acidification theories that suggest the importance of nitrogen-based species (specifically, nitric ($HNO_3$) and nitrous ($HNO_2$) acids) on acidification liquids exposed to an air plasma (e.g. [8, 9]). Though the pH does not change appreciable with steam plasma treatment, it should be pointed out that the baseline value after treatment is weakly dependent on input power. At low input powers ~50W, small reduction in pH (i.e. 6.2 to as low as 6.05) is typically observed in the pH while at higher powers ~250W, the pH stays closer to neutral (pH 6.85–6.95). This effect is not well understood though it may be tied to dissolved nitrogen content in the water. Because the local water temperature is higher at the higher powers, then locally, the

concentration of gaseous nitrogen is lower thus translating into lower acidification. In general, the self-ionization of water becomes important when the concentration of protons ($H^+$) is less than $3 \times 10^{-7}$, which roughly corresponds to pH values of 6.5 and greater. The dissociation of water is given as

$$H_2O(l) \rightleftharpoons H^+(aq) + OH^-(aq) \quad (9)$$

As free protons do not exist in water, equation (9) may also be written as

$$2H_2O(l) \rightleftharpoons H_3O^+(aq) + OH^-(aq) \quad (10)$$

At 25 °C, the water dissociation constant, Kw, is $1.01 \times 10^{-14}$ where Kw = [H3O+][OH−] [31]. As the pH of the water treated with the steam plasma consistently falls in the range of pH 6 to 7, one should be mindful of the autoionization of water, as it can be a significant factor in the pH dynamics of the system. Analysis of possible formation of weak acids and detailed investigation into the pH chemistry is left to future work.

*Conductivity*

Conductivity is a measure of the capacity of the water sample under test to conduct electricity. The finite conductivity is in large part due to the presence of ions in solution derived from the disassociation of salts or acids. The conductivity of the treated water—regardless of whether it was treated with a steam or an air plasma—increased with processing time (see figure 13). This result is somewhat surprising as conductivity can be significantly linked to pH due to the sensitivity of conductivity measurements on the concentration of hydrogen and are usually assumed to be a result of acidification [10]. The result suggests that electrolytic processes at the electrode may be to blame. For example, the dissolution of metal into the liquid would result in a measurable conductivity change. This can occur with copper

electrodes [15]. Here the mechanism involves the formation of carbonic acid owing to the presence of residual oxygen and carbon dioxide in the water. The carbonic acid can remove the oxide layer exposing ionic copper, which would then dissolve into the liquid, thereby increasing the conductivity. Because the remarkable similarities in conductivity between steam and air discharges, it is entirely possible that the observed changes for both discharges is due to this electrode ion dissolution effect. Alternatively, the increased conductivity may be due to the chemistry of the steam discharge. The mobility of $H^+$ in water is the highest of any ion ($36.25 \times 10{-}4\ cm^2\ (s\ V)^{-1}$), which gives protons the highest impact on conductivity measurements (hydroxide ion mobility is $20.62 \times 10{-}4\ cm^2\ (s\ V)^{-1}$, or 57% proton mobility) [32]. This results in hydronium, $H_3O^+$, having a higher mobility than molecules of comparable size [10]. Therefore, the increase in conductivity, regardless of discharge method, may be due to the significant fraction of hydronium formed in the treated liquid. For the steam discharge, the increasing conductivity at nearly constant pH reinforces the idea that complex acid-base equilibrium chemistry is occurring (i.e. the production of some weak acid is occurring to keep the pH between 6 and 7 but the mobility of the acidic protons increases conductivity measurements). The formation of hydronium under electron impact is still somewhat unclear, with several suggested mechanisms under discussion [33]. One commonly accepted reaction chain (may be gas or liquid phase) originates from the electron impact on water, which quickly generates hydronium [32].

$$H_2O + e^- \rightarrow H_2O^+ + 2e^- \quad (11)$$

$$H_2O^+ + H_2O \rightarrow H_3O^+ + OH \quad (12)$$

The formation of $H_3O^+$ can also form hydroxyl radicals, OH (see equation(12)). This highly reactive species (with oxidation potential of 2.80V) is plays a key role via advanced oxidation in sterilization [34] and decomposition [35] processes.

*Nitrate and nitrite concentrations*

Nitrate and nitrite concentrations in both air plasma and steam plasma-treated water samples were measured. These samples were extracted after four minutes of plasma treatment. In the air plasma treated water solution, the concentration of nitrates and nitrites formed in solution was found to be around 100 ppm and 10 ppm, respectively, or ten times the EPA limit for each species for drinking water [36]. The water treated with discharge operating in steam mode, however, was found to have less than 0.5 ppm of nitrate and no nitrite was detected. Without injected gas, the absence of appreciable amounts of nitrogen, such as dissolved content, does not give rise to the production of $NO_x$ species. Indeed, the solubility of nitrogen in water near room temperature is half that of oxygen [31]. This result supports the notion that the pH drop in air discharges in liquid water is most likely due to nitrogen-based acids, especially nitric acid. The absence of $NO_x$ species in steam plasma treated water is desirable for peroxide production. It is well known that nitrites quickly react with $H_2O_2$ in acidic solutions, and can suppress $H_2O_2$ generation, decomposing via [38]

$$N_2O^- + H_2O_2 + H^+ \rightarrow NO_3^- + H_2O + H^+ \quad (13)$$

The very low concentrations of nitrites and nitrates produced in solution in steam plasma treatments as seen in table 1 suggests that this mechanism is not expected to play a role in reducing peroxide production. It should be noted that the water was

not degassed, and the limited quantities of nitrate and nitrite are due to the dissolved gases within the liquid itself.

*Optical emission spectroscopy: steam versus air discharge*

Optical emission spectra were acquired from both the steam and the air fed discharge. The air spectra is dominated by nitrogen emission (figure 14) while the steam plasma emission spectra was found to consist primarily of OH and hydrogen peaks (figure 15). Ozone is not expected to be produced in appreciable levels in the steam discharge. This is in contrast to studies such as [39], which use microwave excitation to form superheated bubbles in which the plasma is ignited. As optical emission spectroscopy of the system does not show any detectable oxygen lines (figure 20), if it assumed ozone is primarily formed through [40]

$$O + O_2 + M \rightarrow O_3 + M \quad (14)$$

ozone production is severely restricted. Ona and Oda [41] observed in a pulsed corona discharge in humid-air an increase in water vapor by 2.4% reduced ozone production by ~6. Indeed, models of dc corona discharges in 100% relative humidity air found ozone suppression by OH [42]:

$$O_3 + OH \rightarrow HO_2 + O_2 \quad (15)$$

This leads to more OH by HO2 recombination [43]:

$$HO_2 + HO_2 \rightarrow H_2O_2 + O_2 \quad (16)$$

It is important to note that Foster et al [12] observed weak O I lines (at 777 nm) during the initial observation of the steam discharge. While not observed in these

studies, oxygen atoms will combine with ozone and water molecules, further preventing ozone production [44]:

$$3\,O + O_3 \rightarrow O_3 + O_3 \quad (17)$$

$$O + H_2O \rightarrow OH + OH \quad (18)$$

Because of this chemical interaction and similar observations (e.g. [45]), strengthened with the fact that the ionizing medium of the discharge itself is water vapor, we do not expect ozone production of any significance in this discharge. Ozone generation was not measured in either discharge. The gas temperature was found through simulating thermal distribution of the OH(A-X) band via LIFBASE spectroscopy software [46], and comparing theoretical results to experimentally observed lines. The gas temperature was found to be approximately 2800 K [13]. A detailed investigation into the time resolved emission spectroscopy of the steam discharge plasma in deionized water may be found elsewhere [13]. At the measured gas temperatures (~2800 K), thermal dissociation of water producing OH and H starts to become significant ($H_2O + H_2O \rightarrow OH + H + H_2O$; $k(T_{gas} = 2800K) \approx 10^{-18}$ - $10^{-16}$ $cm^3$ $s^{-1}$ [47]). Computational models by Bruggeman and Schram [48] suggest production of OH by thermal dissociation becomes comparable to electron dissociation at gas temperatures of 3000 K and greater, though for electron temperatures of 1–2 eV, many authors given the reaction rate of electron dissociation of water a several orders of magnitude above thermal dissociation (where $H_2O + e- \rightarrow OH(X) + H + e-$ ; $k(T_e = 1\text{-}2\ eV) \approx 10^{-12}$ $10^{-10}$ $cm^3$ $s^{-1}$ [48, 49]).

*Hydrogen peroxide production*

As discussed previously, optical emission spectra suggests the steam discharge consists of OH, $H_\alpha$, $H_\beta$, and electrode material (see figure 15). Therefore, it is assumed the steam discharge decomposes contaminants primarily through OH species and hydrogen peroxide, and any reactive daughter products. Nearly exclusive production of OH and $H_2O_2$ makes the steam discharge ideal for oxidation and sterilization applications. The discharge was operated at various power levels in 50mL of deionized water (starting pH = 6.9 ± 0.1, conductivity = 8 ± 1 $\mu Scm^{-1}$). The formation rate of hydrogen peroxide was found to increase with deposited power, as seen in figure 16. These generation rates of hydrogen peroxide are comparable to rates reported in the literature and may be substantially larger to other plasma sources reported in literature. Figure 16 gives an overview of several different plasma sources and the reported hydrogen peroxide formation rates.

**Results: decomposition efficacy of steam discharge to treat Methylene blue dye**

To study the decomposition efficiency of the steam discharge, the discharge was configured to decompose a wastewater simulant. The wastewater simulated contained 0.1mM of methylene blue dye, an organic dye. This dye has been used in the past to study plasma decomposition efficiency of organic contaminants [5, 22, 35, 19]). Discharge operating conditions were varied for each source (i.e. air and steam discharges). The steam discharge was operated at (a) similar and (b) greater than the operating power of the air discharge. The various discharges were operated until (a), similar levels of degradation were achieved (as inferred from spectrophotometric absorbance measurements), and (b), for various time scales.

*Decomposition rates and power levels*

The percentage of methylene blue decomposed by all methods was determined spectrophotometrically, using the reduction in absorbance of a methylene blue absorbance line (609 nm) to track decomposition. Steam discharge treatment of the MB solution was performed at two different relative power levels and compared to an air discharge treatment (see table 2). Preliminary results give the maximum energy efficiency to achieve 50% dye destruction (i.e. the $G_{50}$ value) measured by the steam plasma is around 0.16 g kW $h^{-1}$. This is in comparison to the air discharge, which can achieve $G_{50}$ efficiencies of over 5 g $kWh^{-1}$. This difference of an order of magnitude is recognized in the decomposition parameters. For comparable operating powers (air and steam at approximately 75W), the steam discharge required roughly 7.5 times longer processing time to achieve similar reduction levels (~34min versus ~15min). Increasing the steam discharge power (to 117W and 200W) only increases the $G_{50}$ value of the process slightly to 0.16. It is expected that the air discharge is a more efficient decomposition driver as it has a greater number of reactive species that contribute to the decomposition ability of the air discharge, e.g. such as RNS; this is reflected in the $G_{50}$ value. However, the steam discharge is still attractive the pH levels are kept roughly neutral. Additionally, $G_{50}$ values of 0.16 g kW $h^{-1}$ are similar or an order of magnitude larger than other plasma discharges, such as glow discharge electrolysis and diaphragm discharges [2]. In addition, as the reduction in pollutant is an initially rapid process, using the steam discharge as a pretreatment to initiate pollutant decomposition and not as the sole driver of decomposition would decrease the energy cost while retaining specific decomposition chemistry.

*pH*

The changes of pH over time for the treatment of the methylene blue (MB) dye solution by both the steam and air discharges for both power levels mimicked the results seen with treatment of deionized water (see figure 12). When processed with the air discharge, the MB solution pH drops off exponentially (see figure 17). The solution treated with the steam discharge, on the other hand, did not experience a drop in pH, but instead stayed relatively neutral and unchanged throughout processing time (see figure 17). From a plasma water purification perspective, this result suggests that the steam discharge has the ability to breakdown contaminants without creating highly acidic solutions or decomposition intermediates. It also suggests that the final pH of the processed solution is more dependent on the feed gas used in the discharge and not on the contaminant being treated.

*Conductivity*

As previously seen with plain DI water, the conductively of the MB solution rose with treatment time regardless of discharge type (see figure 18 below). Again, the rise in conductivity can be a function of the increase in hydronium in the system (see the previous section for discussion). Furthermore, through the process of advanced oxidation, the MB is decomposed into small constituent molecules, which can also contribute to the overall solution conductivity.

*Decomposition dynamics: continued destruction post-treatment*

Solutions treated with the steam discharge continue to decompose after the liquid has been subjected to the discharge. 100mL of 0.115mM of Methylene Blue dye solution was treated with the steam discharge for 5min. The decomposition curve of this treatment is shown figure 19, where 63% reduction in dye concentration (as determined via spectrophotometer) was achieved after 300 s of processing via

steam discharge at approximately 200W. After steam plasma treatment, the solution was sealed from the ambient environment and left to age. After 14 d, the aged liquid was found to have a MB concentration of $6.2 \times 10^{-3}$ mM. This corresponds to a further reduction in MB concentration over the 14 d period of over 85%, and a total reduction of MB concentration of over 94% (from 0.11mM to $6.2 \times 10^{-3}$ mM). The physical effect on the treated dye solution may be seen in figure 20. This continued decomposition is assumed to be due to the produced hydrogen peroxide. Immediately after the 5min of steam discharge treatment, the solution contained more than 3% hydrogen peroxide. After the 14 d aging period, the solution contained no detectable hydrogen peroxide.

**Conclusion**

The development of an underwater DBD plasma jet that self-generates a gas bubble of water vapor has been described and studied. This so-called steam discharge is of great interest especially to plasma-based water purification applications, as the system does not require an external feed gas to produce the discharge, which simplifies the operation. In addition, strong decomposition power is retained while the acidity of the liquid is not significantly increased as in other plasma sources (e.g. air fed discharges). This relatively non-acidic pH is also observed during the decomposition of methylene blue dye, suggesting that the pH of the liquid is more strongly dependent on the feed gas used and not the dye by-products. Energy efficiency of the steam discharge on removing methylene blue dye is measured at approximately 0.16g kW $h^{-1}$. Optical emission spectroscopy and hydrogen peroxide measurements suggest the primary source of oxidative strength was derived from OH. Chemical analysis of treated samples indicated that the discharge produces

copious amounts of hydrogen peroxide. These rates matched or exceeded plasma generated rates reported on in the literature to date. The lack of observed oxygen emission lines suggests ozone is not formed in substantial amounts and does not contribute to the decomposition power of the discharge. The steam plasma discharge can be used as a test bed standard for plasma in liquid studies where it is desired to minimize the variety of plasma-produced active species so that chemical pathways can be accurately elucidated.

**Acknowledgments**

This work was supported in part by the National Science Foundation under Grant CBET 1033141 and Grant CBET 1336375, and in part by the National Science Foundation Graduate Student Research Fellowship under Grant DGE 0718128.

**References**

[1] Locke B, Sato M, Sunka P, Hoffmann M R and Chang J-S 2006 Electrohydraulic discharge and nonthermal plasma for water treatment Ind. Eng. Chem. Res. 45 882–905

[2] Malik M 2010 Water purification by plasmas: which reactors are most energy efficient? Plasma Chem. Plasma Process. 30 21–31

[3] Yang Y, Cho Y I and Fridman A 2012 Plasma Discharge in Liquid: Water Treatment and Applications (Boca Raton, FL: CRC)

[4] Pavlovich M J, Chang H-W, Sakiyama Y, Clark D S and Graves D B 2013 Ozone correlates with antibacterial effects from indirect air dielectric barrier discharge treatment of water J. Phys. D: Appl. Phys. 46 145202

[5] Foster J E, Sommers B S, Gucker S N, Blankson I M and Adamovsky G 2012 Perspectives on the interaction of plasmas with liquid water for water purification IEEE Trans. Plasma Sci. 40 1311–23

[6] Kim K-S, Yang C-S and Mok Y S 2013 Degradation of veterinary antibiotics by dielectric barrier discharge plasma Chem. Eng. J. 219 19–27

[7] Traylor M J et al 2011 Long-term antibacterial efficacy of plasma-activated water J. Phys. D: Appl. Phys. 44 472001

[8] Lukes P, Dolezalova E, Clupek I and Sisrova M 2014 Aqueous-phase chemistry and bactericidal effects from an air discharge plasma in contact with water: evidence for the formation of peroxynitrite through a pseudo-second-order post-discharge reaction of H2O2 and HNO2 Plasma Sources Sci. Technol. 23 015019

[9] Oehmigen K et al 2010 The role of acidification for antimicrobial activity of atmospheric pressure plasma in liquids Plasma Process. Polym. 7 250–7

[10] Burlica R, Kirkpatrick M J and Locke B R 2006 Formation of reactive species in gliding arc discharges with liquid water J. Electrostat. 64 35–43

[11] Porter D, Poplin M D, Holzer F, Finney W C and Locke B R 2009 Formation of hydrogen peroxide, hydrogen, and oxygen in gliding arc electrical discharge reactors with water spray IEEE Trans. Ind. Appl. 45 623–9

[12] Foster J E, Weatherford B, Gillman E and Yee B 2010 Underwater operation of a DBD plasma jet Plasma Sources Sci. Technol. 19 025001

[13] Garcia M C, Gucker S N and Foster J E 2015 Understanding the plasma and power characteristics of a Self-generated steam bubble discharge J. Phys. D: Appl. Phys. 48 355203

[14] Maximov A I 2007 Physics, chemistry and applications of the ac diaphragm discharge and related discharges in electrolyte solutions Contrib. Plasma Phys. 47 111–8

[15] Bruggeman P and Leys C 2009 Non-thermal plasmas in and in contact with liquids J. Phys. D: Appl. Phys. 42 053001

[16] Stalder K R, Woloszko J, Brown I G and Smith C D 2001 Repetitive plasma discharges in saline solutions Appl. Phys. Lett. 79 4503

[17] Shih K-Y and Locke B R 2009 Effects of electrode protrusion length, pre-existing bubbles, solution conductivity and temperature, on liquid phase pulsed electrical discharge Plasma Process. Polym. 6 729–40

[18] Kogelschatz U, Eliasson B and Egli W 1997 Dielectric-barrier discharges. Principle and applications J. Physique IV 7 C4–47

[19] Magureanu M, Piroi D, Gherendi F, Mandache N B and Parvulescu V 2008 Decomposition of methylene blue in water by corona discharges Plasma Chem. Plasma Process. 28 677–88

[20] Maehara T et al 2006 Radio frequency plasma in water Japan. J. Appl. Phys. 45 8864–8

[21] Ishijima T, Sugiura H, Saito R, Toyoda H and Sugai H 2010 Efficient production of microwave bubble plasma in water for plasma processing in liquid Plasma Sources Sci. Technol. 19 015010

[22] Foster J E, Adamovsky G, Gucker S N and Blankson I M 2013 A comparative study of the time-resolved decomposition of methylene blue dye under the action of

a nanosecond repetitively pulsed dbd plasma jet using liquid chromatography and spectrophotometry IEEE Trans. Plasma Sci. 41 503–12

[23] Klimiuk E, Kabardo K, Gusiatin Z and Filipkowska U 2005 The adsorption of reactive dyes from mixtures containing surfactants onto Chitin Pol. J. Environ. Stud. 14 771–80

[24] Sahni M and Locke B R 2006 Quantification of hydroxyl radicals produced in aqueous phase pulsed electrical discharge reactors Ind. Eng. Chem. Res. 45 5819–25

[25] Graves D B 2012 The emerging role of reactive oxygen and nitrogen species in redox biology and some implications for plasma applications to medicine and biology J. Phys. D: Appl. Phys. 45 263001

[26] Locke B R and Shih K-Y 2011 Review of the methods to form hydrogen peroxide in electrical discharge plasma with liquid water Plasma Sources Sci. Technol. 20 034006

[27] Gucker S, García M, Yee B and Foster J 2012 Time resolved spectroscopy: dynamic study of a dielectric barrier discharge plasma 65th Annual Gaseous Electronics Conf. (Austin, TX, 2012)

[28] Gucker S N, Yee B and Foster J E 2013 Plasma treatment of contaminated liquid water: a comparison between steam bubble and gas bubble discharge Abstracts IEEE Int. Conf. on Plasma Science (ICOPS) (San Francisco, CA, 2013)

[29] Burlica R, Kirkpatrick M J, Finney W C, Clark R J and Locke B R 2004 Organic dye removal from aqueous solution by glidarc discharges J. Electrostat. 62 309–21

[30] Gucker S N and Foster J E 2011 Power studies of an underwater DBD plasma 38th IEEE Int. Conf. on Plasma Science (Chicago, IL, 2011)

[31] Haynes W M 2013–2014 CRC Handbook of Chemistry and Physics 94th edn (Boca Raton, FL, USA: CRC Press)

[32] Agmon N 2000 Mechanism of hydroxide mobility Chem. Phys. Lett. 319 247–52

[33] Cole C R, Champion Outlaw R A, Baker D H and Holloway B C 2004 Contribution and origin of H3O+ in the mass spectral peak at 19 amu J. Vac. Sci. Technol. A 22 2056

[34] Wk. Lee H et al 2013 Synergistic sterilization effect of microwave-excited nonthermal Ar plasma, H2O2, H2O and TiO2, and a global modeling of the interactions Plasma Sources Sci. Technol. 22 055008

[35] Malik M and Ghaffar A 2001 Water purification by electrical discharges Plasma Sources Sci. Technol. 10 82–91

[36] US Environmental Protection Agency 2009 National primary drinking water regulations EPA, EPA 816-F-09-004

[37] Foster J E, Sommers B and Gucker S 2015 Towards understanding plasma formation in liquid water via single bubble studies Japan. J. Appl. Phys. 54 01AF05

[38] Anbar M and Taube H 1954 Interaction of nitrous acid with hydrogen peroixde and with water J. Am. Chem. Soc. 76 6243–7

[39] Nomura S et al 2011 Characteristics of in-liquid plasma in water under higher pressure than atmospheric pressure Plasma Sources Sci. Technol. 20 034012

[40] Eliasson B and Kogelschatz U 1991 Modeling and applications of silent discharge plasmas IEEE Trans. Plasma Sci. 19 309

[41] Ono R and Oda T 2003 Dynamics of ozone and OH radicals generated by pulsed corona discharge in humid-air flow reactor measured by laser spectroscopy J. Appl. Phys. 93 5876

[42] Chen J H and Wang P X 2005 Effect of relative humidity on electron distribution and ozone production by dc coronas in air IEEE Trans. Plasma Sci. 33 808–12

[43] Moller D 2009 Atmospheric hydrogen peroxide: evidence for aqueous-phase formation from a historic perspective and a one-year measurement campaign Atmos. Environ. 43 5923–36

[44] Lukes P, Appleton A T and Locke B R 2004 Hydrogen peroxide and ozone formation in hybrid gas–liquid electrical discharge reactors IEEE Trans. Ind. Appl. 40 60–7

[45] Nojima H et al 2007 Novel atmospheric pressure plasma device releasing atomic hydrogen: reduction of microbialcontaminants and OH radicals in the air J. Phys. D: Appl. Phys. 40 501–9

[46] Luque J and Crosley D R 1999 LIFBASE: Database and spectral simulation (version 1.5) SRI International Report MP 99-009

[47] NIST Chemical Kinetics Database. NIST Standard Reference Database 17, Version 7.0 (Web Version), Release 1.6.8, Data version 2013.03. [Online]. (http://kinetics.nist.gov/)

[48] Bruggeman P and Schram D C 2010 On OH production in water containing atmospheric pressure plasmas Plasma Sources Sci. Technol. 19 045025

[49] Itikawa Y and Mason N 2005 Cross sections for electron collisions with water molecules J. Phys. Chem. Ref. Data 34 1

[50] Aristova NA and Piskarev I M 2002 Characteristic features of reactions initiated by a flash corona discharge Technol. Phys. 47 1246

[51] Ognier S, Iya-sou D, Fourmound C and Cavadias S 2009 Plasma Chem. Plasma Proc. 29 261–73

[52] Mark G et al 1998 OH-radical formation by ultrasound in aqueous solution—Part II: Terephthalate and Fricke dosimetry and the influence of various conditions on the sonolytic yield Ultrasonics Sonochem. 5 41–52

[53] Thagard S M, Takashima K and Mizuno A 2009 Plasma Chem. Plasma Process. 29 455–73 [

54] Wakeford C A, Blackburn R and Lickiss P D 1999 Ultrasonics Sonochem. 6 141–8 [55] Nikiforov A Y and Leys C 2007 Plasma Sources Sci. Technol. 16 273–80

[56] Stara Z and Krcma F Czech. J. Phys. 54 C1050–C5

[57] Lukes P, Clupek M, Sunka P, Babicky V and Janda V 2002 Effect of ceramic composition on pulse discharge induced processes in water using ceramic-coated wire to cylinder electrode system Czech. J. Phys. 52 D800

[58] Potocky S, Saito N and Takai O 2009 Thin Solid Films 518 918–23

[59] Gao H et al 2008 Analysis of energetic species caused by contact glow discharge electrolysis in aqueous solution Plasma Sci. Technol. 10 30–8

[60] Sato T and Furui T 2010 Characteristics of a plasma flow generated in pure water vapor at atmospheric pressure and its sterilization efficacy Int. Workshop on Plasmas with Liquids (Matsuyama, Ehime, Japan, 2010)

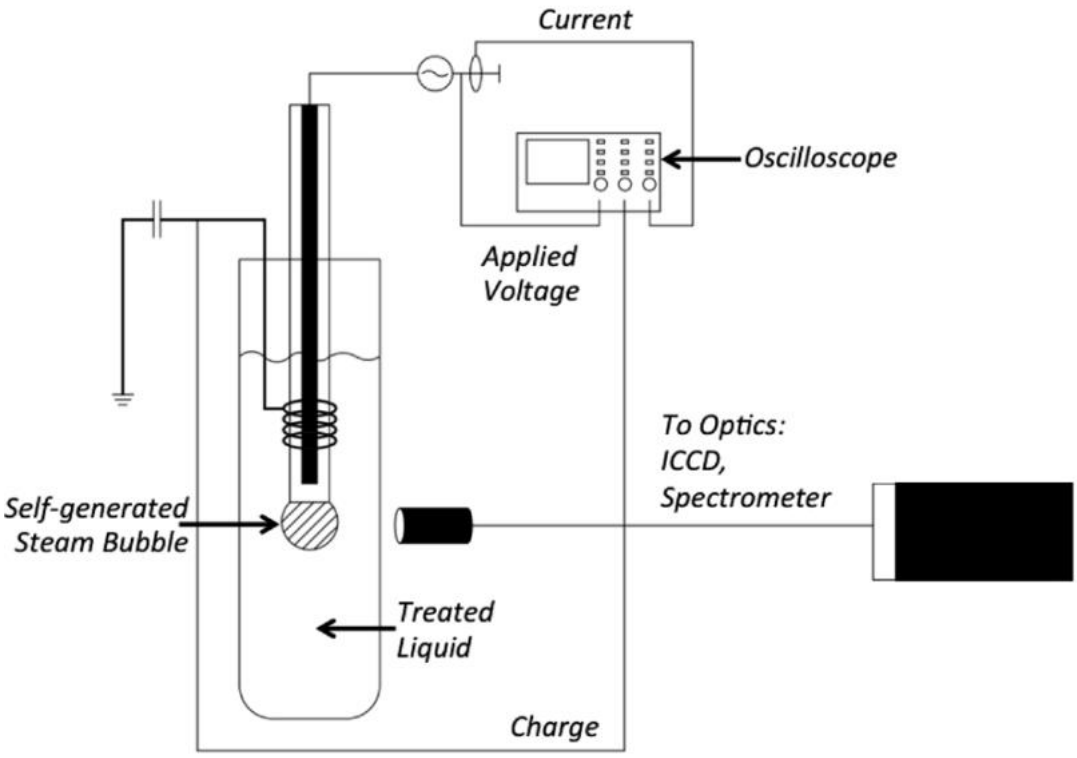


**Figure 1.** Experimental set up

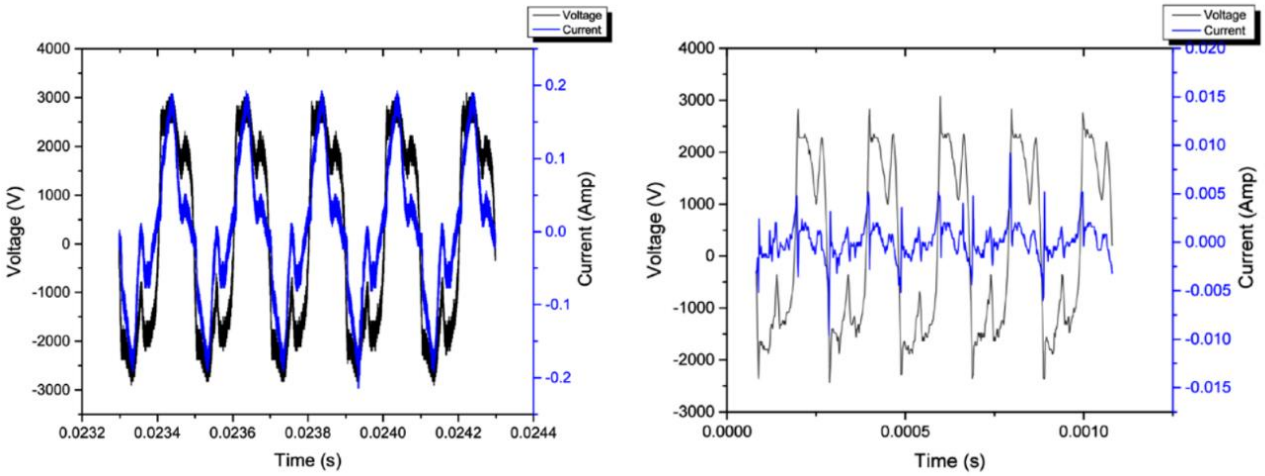


**Figure 2.** Typical voltage and current of the steam discharge (left) and air discharge (right)

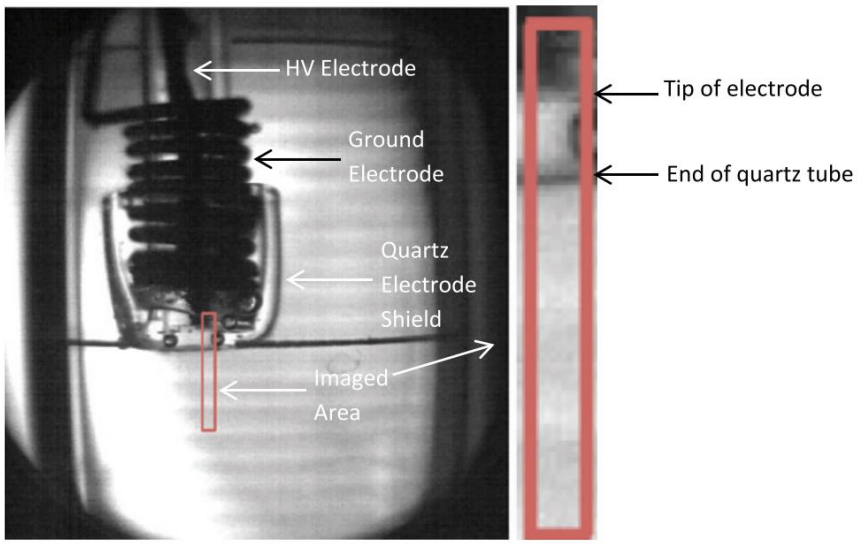


**Figure 3.** Electrode set up with imaged area highlighted (shielded electrode housing design).

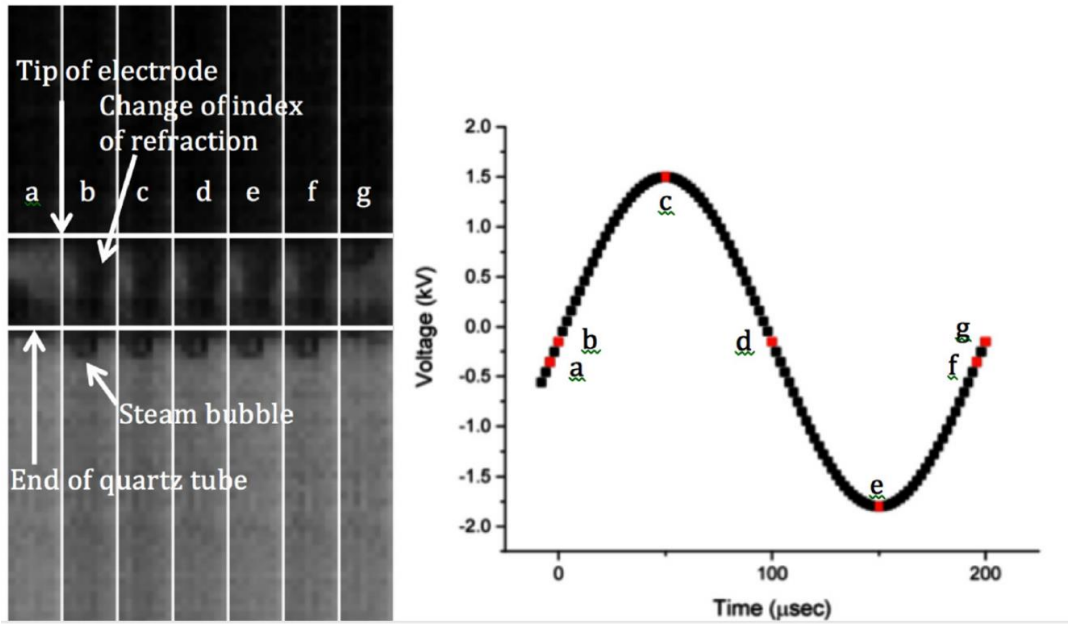


**Figure 4.** From [13]. Early stages of bubble formation. Frames taken over a voltage cycle; (a), taken at −5 µs from the start of the voltage cycle; (b), 0 µs; (c), 50 µs; (d), 100 µs; (e), 150 µs; (f) 195 µs; (g), 200 µs.

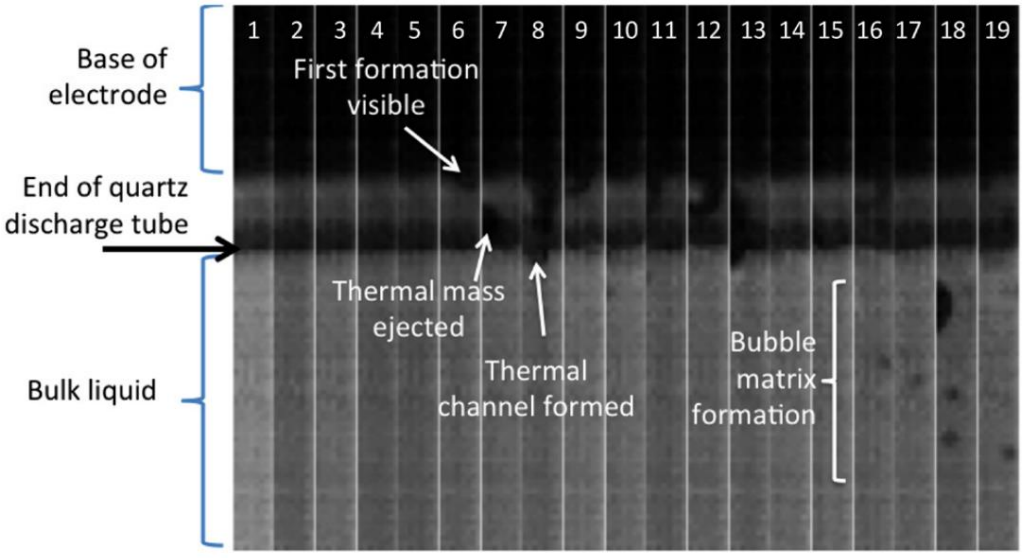


**Figure 5.** Steam bubble formation. Shown t = 0 to t = 3600 µs. Voltage period = 200 µs.

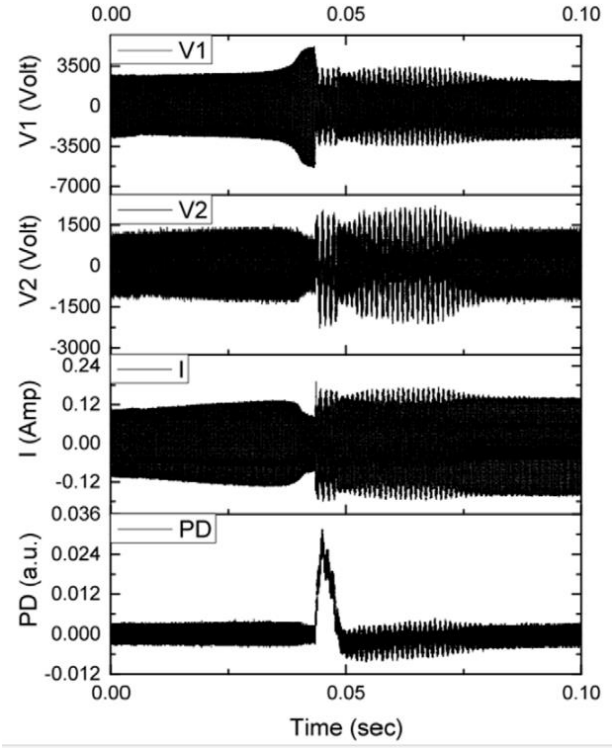


**Figure 6.** Voltage, current and photo diode response of the steam bubble plasma. Bubble formation (0 to ~0.03 s), transition to discharge (~0.03 to ~0.045 s), and plasma discharge (~0.045 s onward) may be observed.

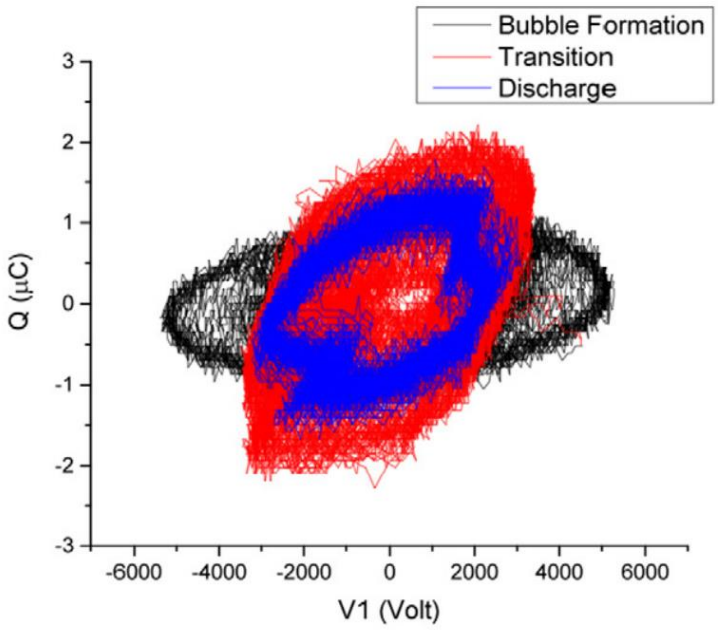

**Figure 7.** Corresponding Lissajous figure for data in figure 6. The different regimes are illustrated in different colors.

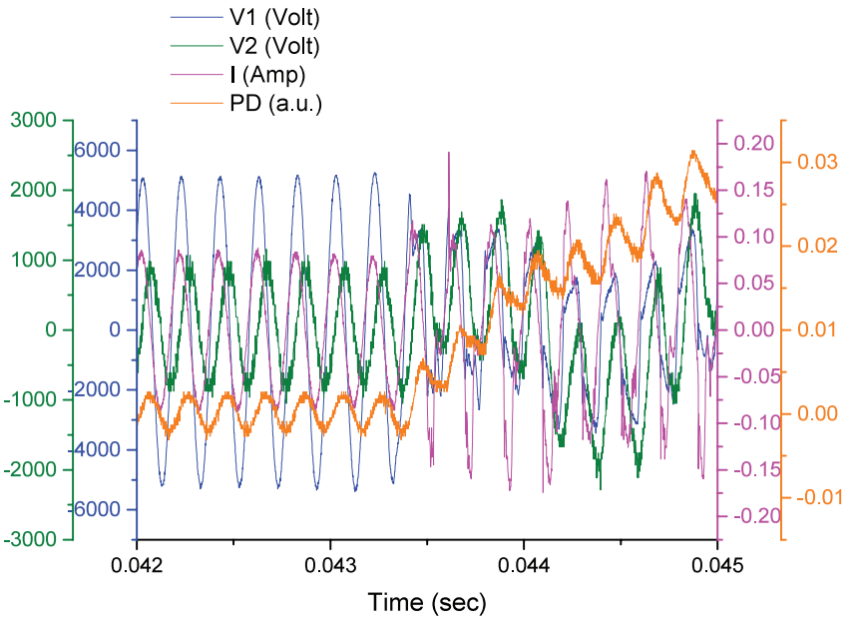


**Figure 8.** The transition region. Applied voltage (V1, blue), voltage across capacitor (V2, green), discharge current (I, pink) and photo diode response (PD in arbitrary units, orange).

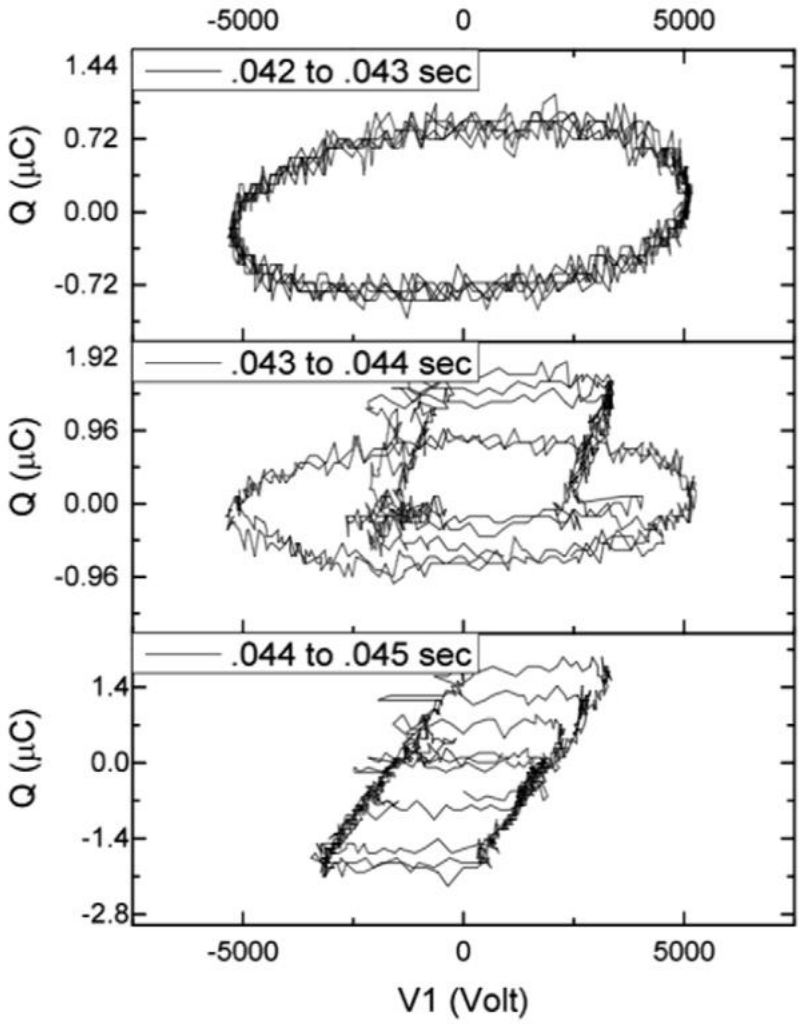


**Figure 9.** Corresponding power deposition from the transition region. Average power for each of the three regions shown above are 71W (top), 75W (middle), and 84W (bottom).

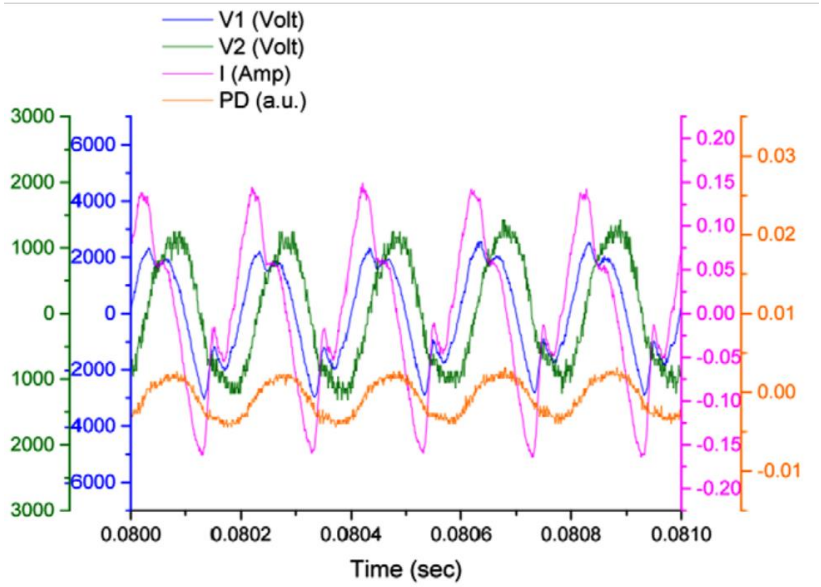


**Figure 10.** The discharge region.

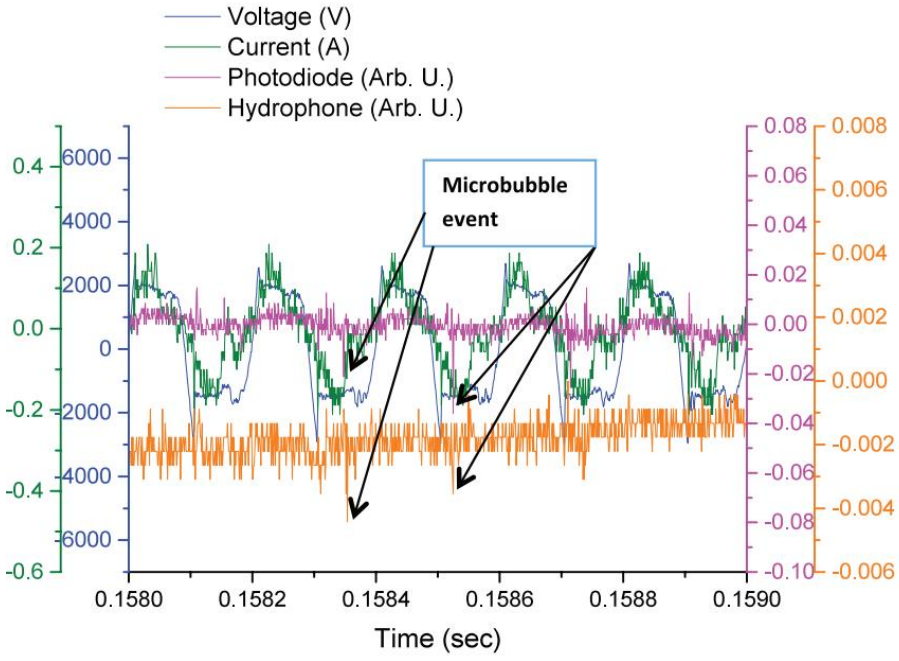


**Figure 11.** Discharge region. Here, the hydrophone is in sync with the photodiode's microspike responses to the plasma strikes.

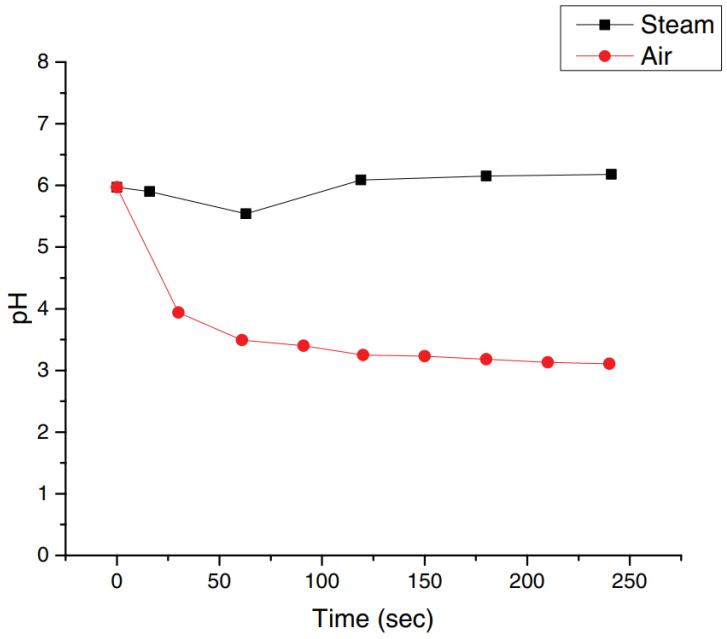


**Figure 12.** Discharges in DI water. Typical pH as a function of time for air (red) and steam (black) discharges.

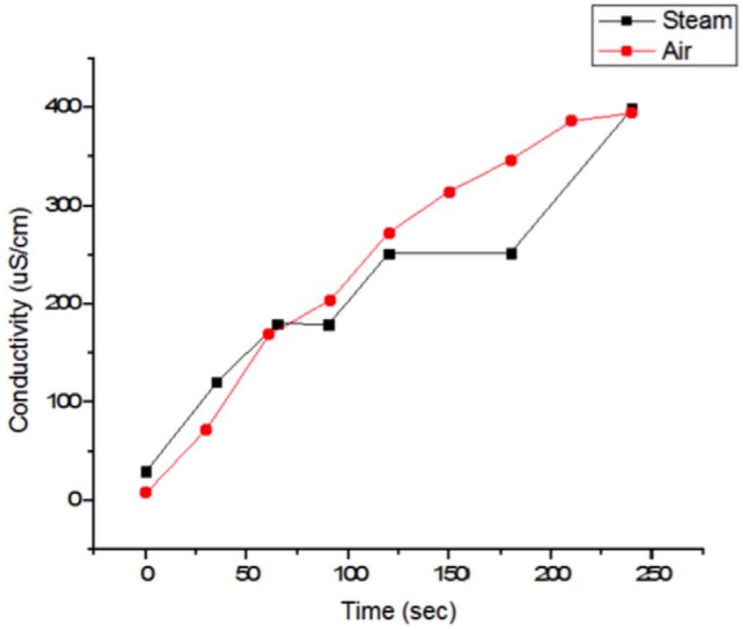


**Figure 13.** Discharges in DI water. Typical conductivity as a function of time for air (red) and steam (black) discharges.

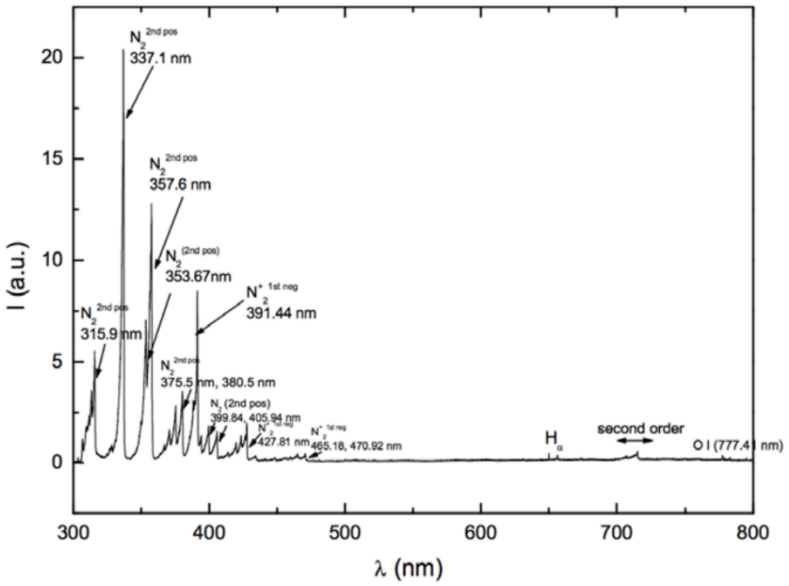


**Figure 14.** Optical emission of air discharge in deionized water. Numerous nitrogen species are visible.

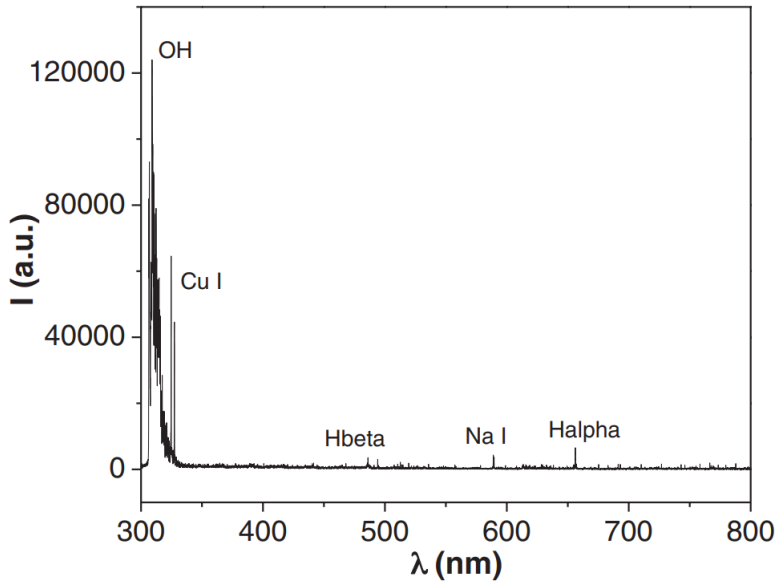


**Figure 15.** Optical emission of steam discharge in deionized water. No nitrogen emission is visible. Copper and sodium lines are emission from the electrode and quartz housing.

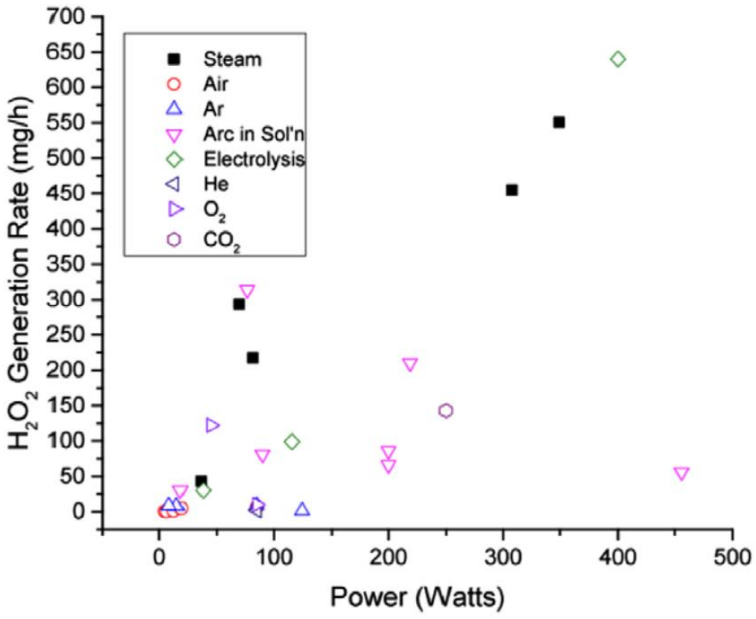


**Figure 16.** Hydrogen peroxide production in various plasma sources [26]. Steam, this paper; Air [50–52]; Argon [52, 53]; Arc in solution [54–57]; Electrolysis [58]; Helium [52]; Oxygen [52, 59]; Carbon dioxide [60].

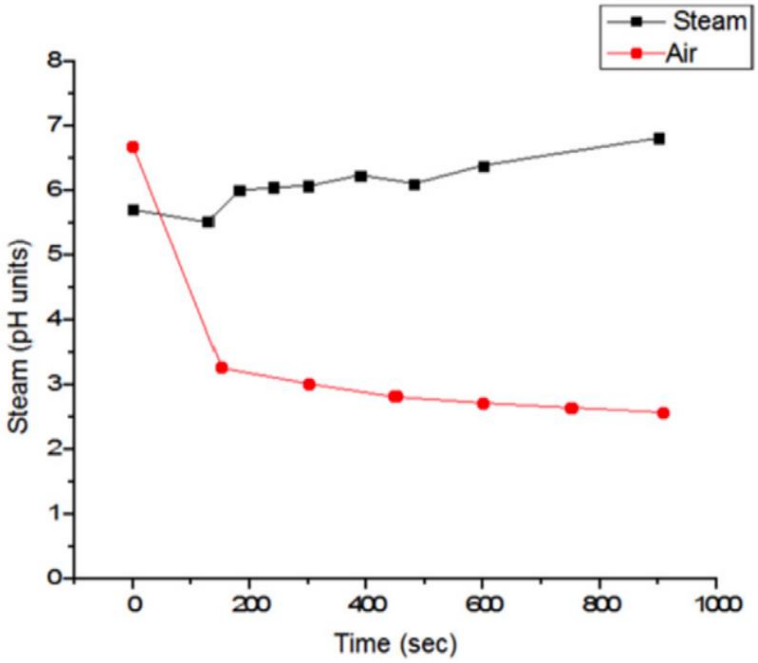


**Figure 17.** pH as a function of time for air (red) and steam (black) discharges in MB solution.

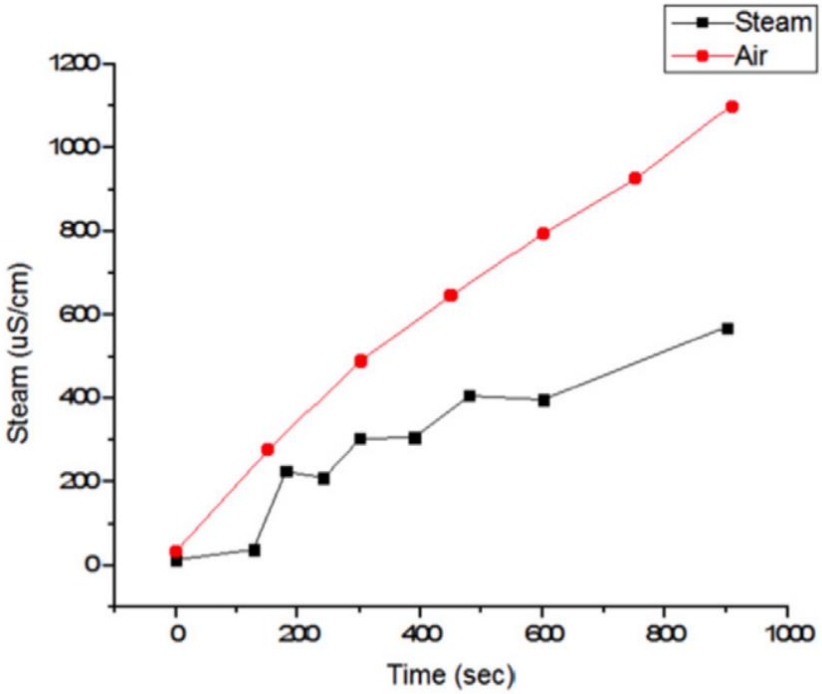


**Figure 18.** Conductivity as a function of time for air (red) and steam (black) discharges in MB solution.

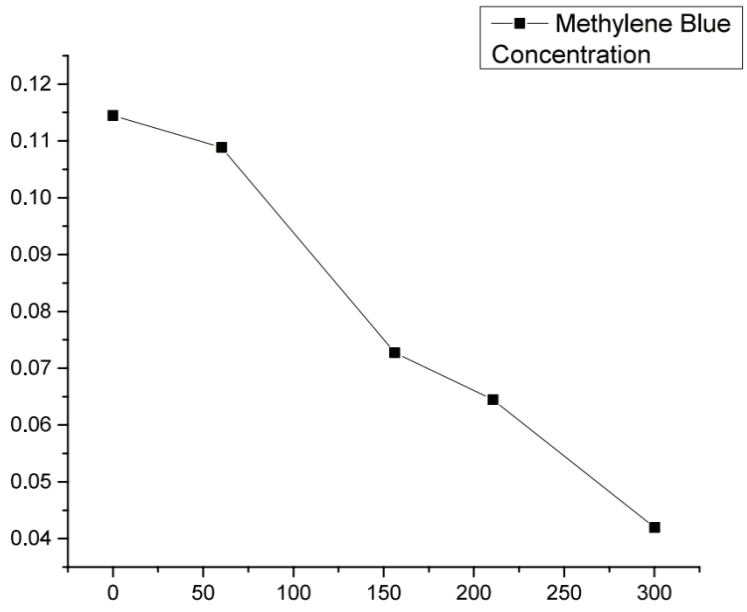


**Figure 19.** Methylene blue concentration reduction over processing time.

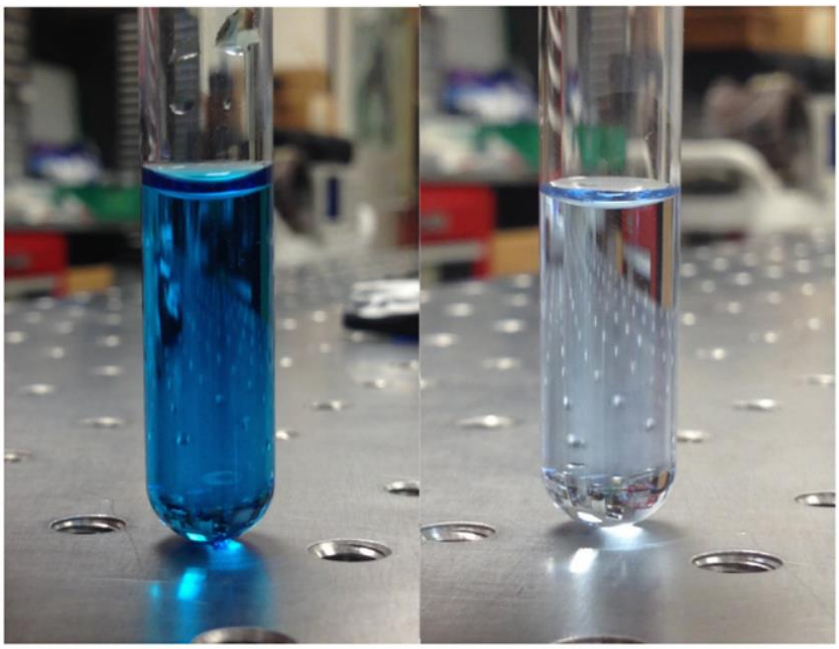

**Figure 20.** The effect of aging on steam-treated MB solutions. Left, solution after 5min of steam treatment. Right, solution after 5min of steam treatment and 14 d of aging.

**Table 1.** Nitrate and nitrite production [37]. Copyright 2015 The Japan society of applied physics.

| | Average nitrate concentration (ppm) | Average nitrite concentration (ppm) |
|---|---|---|
| Untreated DI water | 0.00 | 0.00 |
| DI water treated via air discharge, 4 min | 99.63 | 10.92 |
| DI water treated via steam discharge, 4 min | 0.45 | 0.00 (undetected) |

**Table 2.** Decomposition efficacy of air and steam discharge on MB solution.

| | Deposited power (W) | Treatment time (mm:ss) | Initial/final MB concentration ($\mu$M) | % Reduction | $G_{50}$ Value (g kW $h^{-1}$) |
|---|---|---|---|---|---|
| Air | 75 | 4:30 | 156/3.68 | 97.6 | 5.2 |
| Steam | 76 | 33:42 | 92.5/5.45 | 94.6 | 0.15 |
| Steam | 117 | 15:00 | 92.5/18.05 | 82.0 | 0.16 |
| Steam | 200 | 5:00 | 114/42.0 | 63.3 | 0.16 |